



## Letters

## Ab initio simulations of iron–nickel alloys at Earth's core conditions

Alexander S. Côté\*, Lidunka Vočadlo, John P. Brodholt

Department of Earth Sciences, University College London, Gower Street, London WC1E 6BT, United Kingdom

## ARTICLE INFO

## Article history:

Received 24 October 2011

Received in revised form

8 June 2012

Accepted 14 June 2012

Editor: T. Elliot

Available online 20 July 2012

## Keywords:

iron

nickel

Earth's core

ab initio

## ABSTRACT

We report ab initio density functional theory calculations on iron–nickel (Fe–Ni) alloys at conditions representative of the Earth's inner core. We test different concentrations of Ni, up to ~39 wt% using ab initio lattice dynamics, and investigate the thermodynamic and vibrational stability of the three candidate crystal structures (bcc, hcp and fcc). First of all, at inner core pressures, we find that pure Fe transforms from the hcp to the fcc phase at around 6000 K. Secondly, in agreement with low pressure experiments on Fe–Ni alloys, we find the fcc structure is stabilised by the incorporation of Ni under core pressures and temperatures. Our results show that the fcc structure may, therefore, be stable under core conditions depending on the temperature in the inner core and the Ni content. Lastly, we find that within the quasi-harmonic approximation, there is no stability field for Fe–Ni alloys in the bcc structure under core conditions.

© 2012 Elsevier B.V. All rights reserved.

## 1. Introduction

The exact structure and composition of the Earth's core is still unclear. We know that the primary constituent is iron, but cosmochemical models and meteorite studies suggest that the core must also contain some nickel (Anderson, 1989). Under ambient conditions, iron adopts a body-centred-cubic (bcc) structure. Increasing temperature at ambient pressure causes a transformation to the face-centred-cubic (fcc) phase at ~1150 K. At high pressures (>11 GPa at room temp.) Fe adopts the hexagonal-close-packed (hcp) structure, which persists at Earth's inner core pressures (Stixrude & Cohen 1995; Vočadlo et al. 1997, 1999; Saxena and Dubrovinsky, 2000; Ahrens et al., 2002). However, little information is available on the phase relations of Fe–Ni alloys at core conditions. A relatively low pressure (86 GPa) experimental study by Lin et al. (2002) on a 10% Ni Fe–Ni alloy at temperatures up to 2382 K suggested that while Ni stabilises the fcc phase to higher pressures and lower temperatures, the stable phase at Earth's core conditions would still be the hcp phase. A more recent experimental study by Dubrovinsky (2007) up to 225 GPa and 3400 K suggested that an alloy with 10% Ni would adopt the bcc structure at core conditions. The following year, Kuwayama et al. (2008) carried out an experiment with alloys containing up to ~25% Ni, reaching 300 GPa and 2000 K. Their results suggested that, depending on the abundance of Ni in the outer core in the early core formation period, the inner core should be in the hcp or fcc structure, and they found no evidence of bcc. The above uncertainty has prompted this ab initio study,

where we use lattice dynamics to probe the structure of Fe–Ni alloys of different concentrations at pressures and temperatures representative of the Earth's inner core (up to 330 GPa and 5500 K).

Finding the correct crystal structure of the inner core is very important for understanding the observed seismic anisotropy and it would provide a crucial constraint in recent Earth models. More specifically, we know that the elastic anisotropy depends on the particular crystal alignment, therefore different inner core phases will naturally result in different amounts of anisotropy. Furthermore, recent inner core models (Alboussière et al., 2010; Monnereau et al., 2010; Gubbins et al., 2011) suggest different mechanisms of inner core evolution which depend on the particular rheology, mass convection and heat flow in the inner core. These properties are largely dependent on the choice of crystal structure in the inner core since interpreting the anisotropy in terms of flow requires knowledge of that crystal structure. A convecting core would line up to the flow direction in a particular way, and incorrect assumptions about the structure would give rise to a different elastic anisotropy from the one observed. We have shown in previous studies (Vočadlo et al., 2003; Côté et al., 2010) that temperature has an important influence on the inner core's structure, so using lattice dynamics we have the opportunity, within the quasi-harmonic approximation, to examine the phase relations between the candidate phases of Fe–Ni alloys at core conditions.

## 2. Computational methods

The Density Functional Theory (DFT) calculations in this work were carried out using the VASP code (Kresse and Furthmüller, 1996), using the generalised gradient approximation (GGA)

\* Corresponding author. Tel.: +44 20 7679 2425; fax: +44 20 7679 2685.  
E-mail address: a.cote@ucl.ac.uk (A.S. Côté).

(Wang and Perdew, 1991) to represent the exchange–correlation energy. VASP calculates the ground state ( $T=0$ ) for each set of ionic positions and the electronic free energy is taken as the quantity to be minimised. The  $k$ -point sampling grid and cutoff energies were chosen carefully so that the energy convergence would not exceed 1 meV/atom. Specifically, we used a 400 eV cutoff energy throughout the calculations. For pure iron, the  $k$ -point grid chosen is described in our previous work (Côté et al., 2010). For the Fe–Ni alloys, different concentrations of Ni were achieved by substitution in primitive cells of 4 or 8 atoms. We compared the thermodynamical stability of the fcc and hcp phases using three different concentrations of Ni (12.5%, 25% and 37.5%). Achieving the latter concentration requires three Ni atoms in the 8 atom cell, so a number of trials were performed with all the different configurations of the defect atoms in both phases, and the most favourable configurations at high pressure were chosen. For the fcc supercell, the lowest energy 8-atom structure is the one with the three Ni atoms positioned at coordinates (0,0,0), (0.25,0.75,0.5), and (0.25,0.25,0.5); for the orthorhombic hcp supercell, those coordinates are (0,0,0), (0.25,0.5,0) and (0.5,0,0). The  $k$ -point grids used in the 8 atom cases were  $6 \times 6 \times 12$  for bcc (equivalent to 36  $k$ -points in the irreducible Brillouin zone (IBZ)),  $6 \times 6 \times 9$  for fcc (30  $k$ -point in the IBZ) and  $6 \times 6 \times 6$  for hcp (64  $k$ -points in the IBZ). Correspondingly dense grids were used in the 25% hcp and low bcc concentrations where 4- and 16-atom primitive cells were used respectively.

We calculated the phonon frequencies for different structures and examined their vibrational stability. The phonon calculations were carried out using the code PHON (Alfè, 1998), which calculates the phonon vibrational frequencies  $\omega_{ks}$  along a pre-defined path in the 1st Brillouin zone, by using the small displacement method to construct force constant matrices.

To get accurate results in the phonon calculations, very accurate forces are needed. We therefore used a very low tolerance criterion for the total energy ( $10^{-7}$  eV), and an added grid in the Fourier transform mesh in order to reduce the noise in the forces, which were set to converge below  $10^{-5}$  eV/Å. The atoms were displaced by a small distance (0.01 Å) from their equilibrium positions, in order for the forces to remain within the harmonic approximation, and the forces were calculated. For all cases, the calculations were performed on supercells large enough to avoid self-interaction due to the periodic boundary conditions, typically three times the size of the primitive unit cell in each direction. The resulting supercells contained up to 288 atoms. We must also note that none of the phonon calculations was spin-polarised. We know that bulk fcc Ni remains ferromagnetic to highest compression, but the Ni concentrations studied here are not high enough for magnetism to persist at high pressures.

Our calculations were extended to nonzero temperatures by using the quasi-harmonic approximation, where the volume and temperature dependence of the Helmholtz free energy  $F(V,T)$  was calculated as a sum of the contributions due to static compression,  $F_0(V)$ , thermal excitation of electrons,  $F_{el}(V,T)$ , and thermal excitation of phonons,  $F_{vib}(V,T)$ :

$$F(V,T) = F_0(V) + F_{el}(V,T) + F_{vib}(V,T) \quad (1)$$

The last term in (1) is defined as

$$F_{vib}(V,T) = k_B T \sum_{s,\mathbf{k}} \ln \left[ 2 \sinh \left( \frac{\hbar \omega_{s\mathbf{k}}}{2k_B T} \right) \right] \quad (2)$$

where  $k_B$  is the Boltzmann constant, and  $\omega_{s\mathbf{k}}$  is the frequency of the phonon mode for wave vector  $\mathbf{k}$  and volume  $V$ .

The contribution to the free energy from electronic excitations at different electronic temperatures  $F_{el}(V,T)$  was included by using a Fermi smearing function when calculating the ground-state

energy in VASP. Adding the electronic temperature makes a big difference in the stability of different phases.

The Gibbs free energy was then obtained by

$$G(P,T) = F(V,T) + PV \quad (3)$$

In order to account for the contribution of thermal pressure at different temperatures and obtain the last term of (3) accurately, we performed free energy calculations at 6 different volumes, corresponding to pressures in the range 200–400 GPa. We then fitted the results to an  $E(V)$  Birch–Murnaghan 3rd order equation of state, from where we were able to find the correct volume for any pressure at various temperatures. The total free energies for core pressures and temperatures could thus be evaluated. Using that  $P$ – $V$ – $T$  data allowed us to construct a thermal equation of state based on Birch–Murnaghan’s 3rd order formulation:

$$P = \frac{3}{2} K_0(T) \left[ \left( \frac{V}{V_0} \right)^{7/3} - \left( \frac{V}{V_0} \right)^{5/3} \right] \left[ 1 + \frac{3}{4} (K'_0 - 4) \left( \left( \frac{V}{V_0} \right)^{2/3} - 1 \right) \right] \quad (4)$$

where  $V_0$  is the temperature dependent zero-pressure volume, linearly approximated as

$$V_0(T) = V_0(T_0) \exp \left( \alpha_0 (T - T_0) + \frac{1}{2} \alpha_1 (T^2 - T_0^2) \right) \quad (5)$$

where  $T_0$  is a reference temperature at which the volume is  $V_0$  and the bulk modulus has the value  $K_0$ . The thermal expansion coefficient varies linearly with temperature as  $a(T) = a_0 + a_1 T$ . With this formulation (Angel, 2001), the actual values of  $\alpha_0$  and  $\alpha_1$  that describe a  $V$ – $T$  curve depend on the value of the reference temperature  $T_0$ .

It should be noted that the calculations are quasi-harmonic and, therefore, neglect anharmonicity, which may be important at high temperatures. It has been shown that the total anharmonic contribution to the free-energy of hcp Fe at 6000 K is only of the order of 60 meV/atom (Alfè et al., 2001). Since fcc is a close-packed structure like hcp, it should have a similar anharmonic contribution. It is thus unlikely for the free-energy differences to be larger than  $\sim 10$  meV/atom, even at very high temperatures, and since it is free-energy differences that are important, anharmonic contributions are unlikely to change phase transition temperatures substantially. We have, therefore, used 10 meV/atom to estimate the uncertainty in the temperature of our predicted hcp–fcc phase transitions. It should be noted, however, that the anharmonic contribution to the free-energy may be higher for the bcc phase, as it is not close-packed. This may lead to larger (and as yet unknown) errors in the temperature of bcc phase transitions. The Ni bearing phases may have more intrinsic anharmonicity than pure Fe, but we currently have no reason to suspect that the difference will be significantly greater than in pure Fe (10 meV/atom).

### 3. Results

#### 3.1. Vibrational stability

We substitutionally inserted different concentrations of nickel at high pressure in all three phases (bcc, fcc and hcp). As reported previously (Côté et al., 2010), the bcc phase of pure iron becomes vibrationally unstable at high pressures above  $\sim 200$  GPa, but the addition of Si stabilises it. Ni, however, does not have the same effect. At low concentrations the bcc structure remains vibrationally unstable, and at concentrations above  $\sim 9\%$ , if the geometry is allowed to relax, it transforms to the fcc structure. Interestingly, this only happens when the electronic temperature corresponds

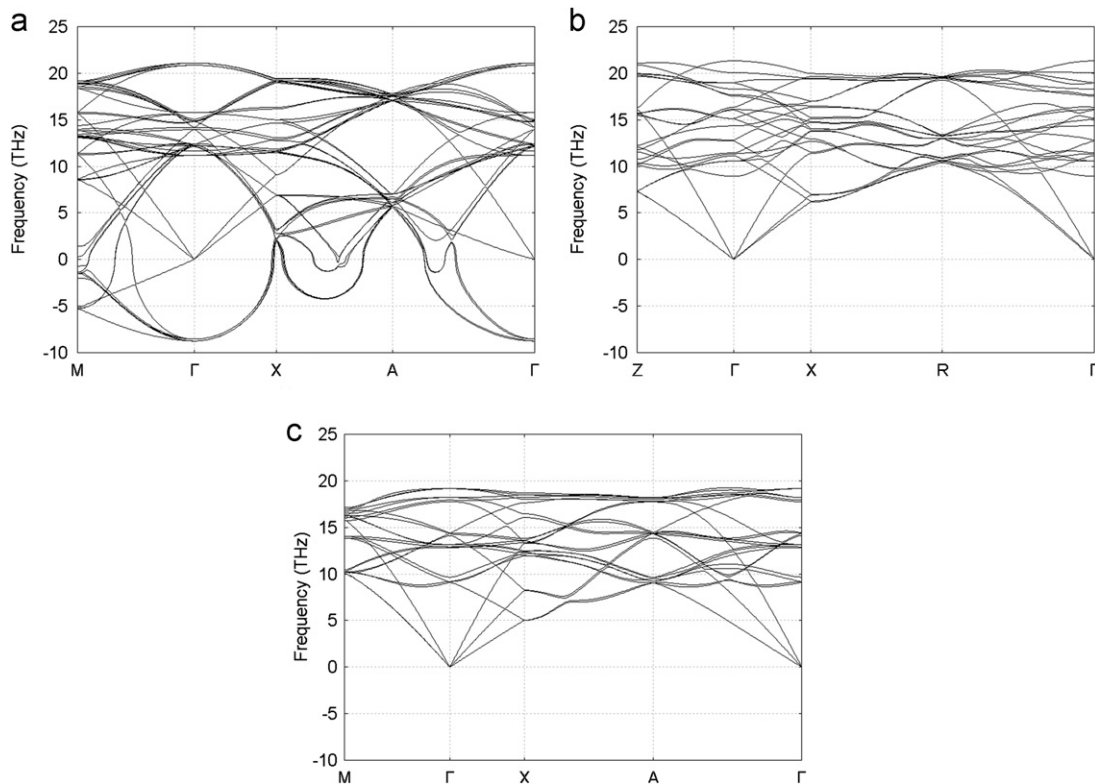


**Fig. 1.** Phonon dispersion relations of Fe–Ni alloys at 330 GPa for (a) 6.25% Ni in the bcc structure, where the mechanical instability is obvious, compared with 12.5% Ni in the (b) fcc and (c) hcp structures. With 12.5% Ni, bcc transforms to fcc after a geometry optimisation.

to core temperatures ( $\sim 5500$  K). Phonon dispersion relations for the different structures are presented in Fig. 1.

At lower electronic temperatures ( $< 4000$  K), the  $\text{Fe}_{0.9}\text{Ni}_{0.1}$  alloy remains in the bcc structure, but, like pure iron, it is vibrationally unstable, at least in the quasiharmonic approximation. Consequently, examining the thermodynamical stability of bcc was not feasible in this study. Previous theoretical studies have pointed out that the bcc phase is dynamically and elastically stable due to anharmonic effects (Vočadlo et al., 2003; Belonoshko et al., 2003; Luo et al., 2010); this work, however, suggests that above 4000 K it would transform to fcc if the Ni concentration is above  $\sim 9\%$ .

Both fcc- and hcp-Fe remain dynamically stable with the addition of Ni. We were therefore able to examine their relative thermodynamical stability at core conditions.

## 3.2. Thermodynamical stability

### 3.2.1. Pure iron

We know that pure iron in the bcc structure is unlikely to become thermodynamically stable at core conditions (Vočadlo et al., 2008a) so we only compare the two remaining phases, fcc and hcp. From our results at all pressures and temperatures we put together the 3D energy diagram which is shown in Fig. 2. As can be seen – assuming that anharmonicity does not affect this – fcc-iron becomes the stable phase even at high pressures, provided that the temperature is high enough, in fact very close to the melting temperature. If the electronic temperature is not correctly applied, the vibrational contribution alone is not enough to stabilise fcc, as was the case with our previous study (Côté et al., 2010). We note that this result does not contradict earlier work on iron phase stability (Vočadlo et al., 2008b) based on calculations at 5500 K, where the hcp phase was predicted to be more stable, in agreement with the results presented here (Fig. 2).

### 3.2.2. Iron–nickel alloy

The Gibbs free energies for the Fe–Ni alloys as a function of temperature at pressures of 200 and 330 GPa are plotted in Fig. 3, relative to the hcp phase. We evaluated the free energies at 200 GPa as well as the inner core pressure, in order to compare our results with the available experimental data. It is clear that both Ni concentration and high temperatures increase the stability field of the fcc phase, with Ni concentration having a smaller effect at high temperatures. As can be seen from Fig. 3, at 37.5% Ni fcc is always the most stable phase. The thermal equations of state (Eq. (4)) using a reference temperature of 6000 K for the different Ni concentrations of fcc and hcp are shown in Table 1.

Using the free energy results, we can estimate the Ni concentration needed for the fcc phase to become the stable phase thermodynamically. To do this, we added the configurational term  $k_B T(c_{\text{Ni}} \ln(c_{\text{Ni}}) + c_{\text{Fe}} \ln(c_{\text{Fe}}))$ , where  $c$  represents the atomic% concentration, to the energies of the individual phases. The resulting solid solution energies were then fitted to a polynomial for each phase, the crossing point of the two lines representing the phase transition. This estimate ignores any solid solutions, and it represents the theoretical pseudo-univariant reaction, where one phase would transform straight into the other. Superimposing our results on the experimentally derived phase diagram of Kuwayama et al. at 200 GPa we obtain Fig. 4. We can see that our pseudo-univariant line is completely consistent with all available experimental data. At higher temperatures we predict a steeper phase transition than suggested by Kuwayama et al., which they obtained by extrapolating their low temperature experimental data to match the pure iron transition temperature by Boehler (2000); the transition temperature we predict for pure iron is  $\sim 500$  K lower.

We attempted to derive a two-phase region around the pseudo-univariant line, however we were unable to use the common tangent technique, described in Côté et al. (2010), due

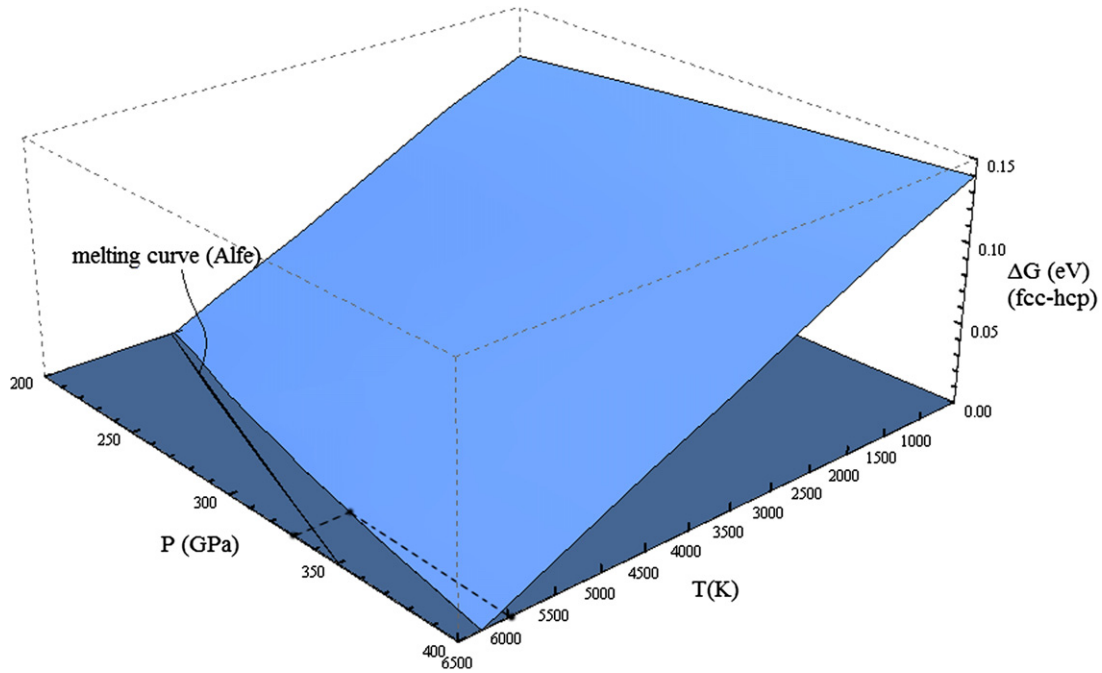


**Fig. 2.** Gibbs free energy of fcc as a function of pressure and temperature with respect to hcp (zero plane). The crossing points of the two planes indicate the point of the phase transition. Specifically at 330 GPa, the required temperature for stabilising fcc is  $\sim 6000$  K, below the melting point of 6300 K, as calculated by Alfe et al. (2002).

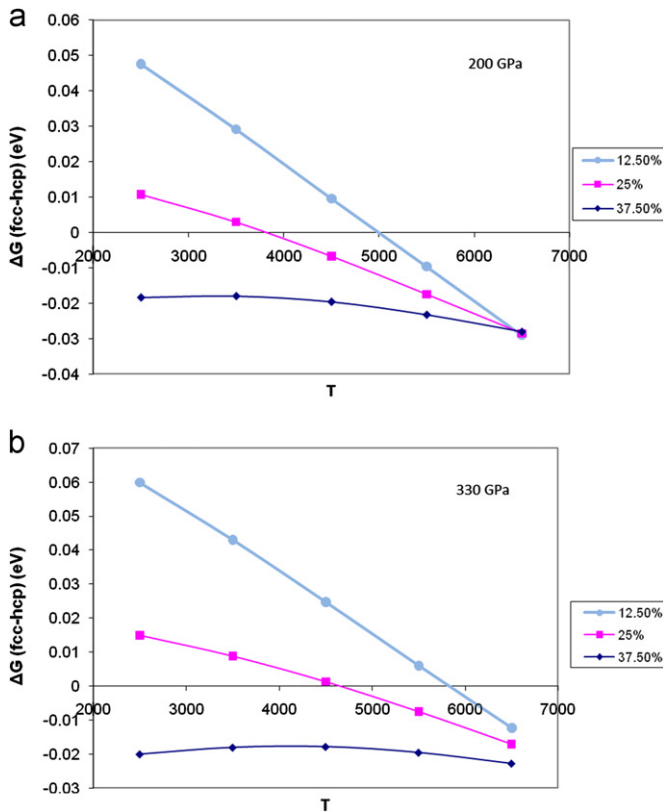


**Fig. 3.** Gibbs free energy difference of fcc with respect to hcp ( $\Delta G=0$  line) vs. temperature at (a) 200 GPa and (b) 330 GPa, for increasing concentrations of Ni. fcc is becoming more stable with respect to hcp with increasing temperature and concentration. The lines through the points are guides for the eye.

to the very small energy difference between the two phases and the almost linear increase of free energy with Ni concentration at 200 GPa. Thus we were not able to determine the exact extent of the two-phase solid solution. The yellow shaded region in Fig. 4 is,

therefore, an estimate based on our calculated two-phase region at the inner core boundary pressure (330 GPa), where the aforementioned technique could be applied, and is depicted in the inset of Fig. 4. The width of our estimated two-phase region at 200 GPa is also consistent with that measured by Kuwayama et al. (2008) at low temperatures. Finally, it is also worth noting that the addition of nickel makes very little difference to the iron phase transition before  $\sim 13$  wt% Ni.

#### 4. Discussion

We find that at 330 GPa the hcp phase of pure iron transforms to the fcc phase at  $\sim 6000$  K. We also find that the presence of nickel lowers this transition temperature, particularly at concentrations of Ni above  $\sim 13\%$ . This result is based on the assumption that there is no significant *difference* in the anharmonic contribution to the Gibbs free energies of the fcc and hcp phases, and also that any additional anharmonic contribution arising from the presence of nickel will be similar for each phase, so that the free energy difference is unaffected. Our result for pure iron is in agreement with the theoretical and experimental results of Mikhaylushkin et al. (2007) and also with earlier ab initio molecular dynamics calculations (Vočadlo et al., 2008b) which predicted that the thermodynamically stable phase of pure iron at 5500 K is the hcp phase (see Fig. 2).

Whether the inner core is in the fcc structure rather than the hcp structure depends on the temperature of the core, the nickel concentration and the light element concentration. For a Fe–Ni core, at temperatures below  $\sim 6000$  K and moderate Ni content ( $\sim 5\%$ ), the core is likely to be in the hcp structure; a hotter core and/or higher Ni concentrations will likely change the core phase to the fcc structure. This transition temperature will be even lower if light elements are taken into account; for example, Côté et al. (2010) have shown that 13 atm% (7 wt%) Si reduces the transition temperature to 5500 K. It is also possible that the core could be a mixture of both phases (Mikhaylushkin et al., 2007; Côté et al., 2010). Our results show that for the Fe–Ni system, very

**Table 1**Thermal equation of state parameters for different concentrations of Ni, for the fcc and hcp crystal structures. Reference temperature  $T_0=6000$  K.

	12.5% Ni		25% Ni		37.5% Ni	
	fcc	hcp	fcc	hcp	fcc	hcp
$V_0/\text{atom}$ ( $\text{\AA}^3$ )	99.9962	99.0594	95.9726	47.6502	96.7767	95.7073
$K_0$ (GPa)	165.3468	170.3889	201.5196	204.7459	190.7421	202.3631
$K'$	4.2170	4.2082	4.0840	4.1035	4.1391	4.0828
$\alpha_0$ ( $\times 10^{-5}$ K)	1.9870	1.9496	1.8689	1.8199	1.8935	1.8659
$\alpha_1$ ( $\times 10^{-8}$ K)	0.4279	0.4237	0.28745	0.2561	0.2755	0.2598
$dK/dT$	-0.0240	-0.0244	-0.0212	-0.0199	-0.0198	-0.0203

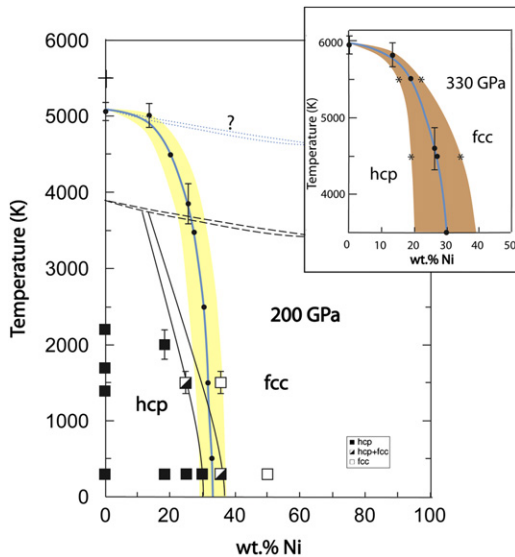


**Fig. 4.** Compositional phase diagram of the Fe–Ni system at 200 GPa, superimposed on the experimental results of Kuwayama et al. (2008). The yellow coloured region indicates an estimated solid solution range based on the experiment, and includes the pseudounivariant (blue line). The pure iron hcp to fcc phase transition happens at a lower temperature than the one estimated by Kuwayama et al. (black cross at  $\sim 5500$  K) which they obtained by extrapolating experimental results of Boehler (2000). The black dashed line denotes an estimated melting curve at 200 GPa starting from Boehler's pure iron melting point assuming very little compositional effect. The dotted blue line is a shift of that melting curve such that it starts at Alfe's ab initio melting point for pure iron at 200 GPa (2002). The inset shows the two-phase loop at 330 GPa, where it was calculated using the common tangent technique (Côté et al., 2010). At 330 GPa the melting point starts higher, at  $\sim 6300$  K. The melting curve has not been estimated. (For interpretation of the references to colour in this figure legend, the reader is referred to the web version of this article.)

high concentrations of Ni and low temperatures are required in order to be in the two-phase region. However, a full analysis is needed that includes light elements in order to quantify this mixed-phase region.

Finally, this study found the bcc phase of iron remains vibrationally unstable with the addition of nickel, making it impossible to calculate any free energies; however, this does not necessarily mean that we can rule the bcc phase out altogether as a candidate for the inner core, as it has been found to be stabilised by light elements (Vočadlo et al., 2003; Côté et al., 2008).

## Acknowledgements

The work of ASC was supported by NERC Grant NE/C519662/1. The computations were performed on the HECTOR service.

## References

- Ahrens, T.J., Holland, K.G., Chen, G.Q., 2002. Phase diagram of iron, revised core temperatures. *Geophys. Res. Lett.* 29 (7), 1150.
- Alboussière, T., Deguen, R., Melzani, M., 2010. Melting-induced stratification above the Earth's inner core due to convective translation. *Nature* 466, 744–747.
- Alfè, D., 1998. PHON: A Program to Calculate Phonons Using the Small Displacement Method. <<http://chianti.geol.ucl.ac.uk/~dario>>.
- Alfè, D., Gillan, M.J., Price, G.D., 2002. Composition and temperature of the Earth's core constrained by combining ab initio calculations and seismic data. *Earth Planet. Sci. Lett.* 195, 91–98.
- Alfè, D., Price, G.D., Gillan, M.J., 2001. Thermodynamics of hexagonal close packed iron under Earth's core conditions. *Phys. Rev. B* 64, 04512316.
- Anderson, D.L., 1989. *Theory of the Earth*. Blackwell Scientific Publications, Boston (pp. 289–305).
- Angel, R.J., 2001. Equations of state. In: Hazen, R.M., Downs, R.T. (Eds.), *High-pressure, High-temperature Crystal Chemistry*. Reviews in Mineralogy and Geochemistry, vol. 41; 2001, pp. 35–60.
- Belonoshko, A.B., Ahuja, R., Johansson, J., 2003. Stability of the body-centred-cubic phase of iron in the Earth's inner core. *Nature* 424, 1032–1034.
- Boehler, R., 2000. High-pressure experiments and the phase diagram of lower mantle and core materials. *Rev. Geophys.* 38, 221–245.
- Côté, A.S., Vočadlo, L., Brodholt, J.P., 2008. Light elements in the core: effects of impurities on the phase diagram of iron. *Geophys. Res. Lett.* 35, L05306.
- Côté, A.S., Vočadlo, L., Dobson, D.P., Alfe, D., Brodholt, J.P., 2010. Ab initio lattice dynamics calculations on the combined effect of temperature and silicon on the stability of different iron phases in the Earth's inner core. *Phys. Earth Planet. Inter.* 178, 2–7.
- Dubrovinsky, L., 2007. Body-centred cubic iron-nickel alloy in Earth's core. *Science* 316, 1880–1883.
- Gubbins, D., Sreenivasan, B., Mound, J., 2011. Melting of the Earth's inner core. *Nature* 473, 361–363.
- Kresse, G., Furthmüller, J., 1996. Efficient iterative schemes for ab initio total-energy calculations using a plane-wave basis set. *Phys. Rev. B* 54, 11,169–11,186.
- Kuwayama, Y., Sawai, T., Hirose, K., Nagayoshi, S., Ohishi, Y., 2008. Phase relations of iron and iron–nickel alloys up to 300 GPa: implications for composition and structure of the Earth's inner core. *Earth Planet. Sci. Lett.* 273, 379–385.
- Lin, J.-F., Heinz, D.L., Campbell, A., Devine, J.M., Mao, W.L., Shen, G., 2002. Iron–nickel alloy in the Earth's core. *Geophys. Res. Lett.* 29, L015089.
- Luo, W., Johansson, B., Eriksson, O., Arapan, S., Souvatzis, P., Katsnelson, I., Ahuja, R., 2010. Dynamical stability of body center cubic iron at Earth's core conditions. *PNAS* 107 (22), 9962–9964.
- Mikhaylushkin, A.S., Simak, S.I., Dubrovinsky, L., Dubrovinskaya, N., Johansson, B., Abrikosov, I., 2007. Pure iron compressed and heated to extreme conditions. *Phys. Rev. Lett.* 99, 1655505.
- Monnereau, M., Calvet, M., Margerin, L., Souriau, A., 2010. Lopsided growth of Earth's inner core. *Science* 328, 1014–1017.
- Saxena, S.K., Dubrovinsky, L.S., 2000. Iron phases at high pressures and temperatures: phase transition and melting. *Am. Mineral.* 85, 372–375.
- Stixrude, L., Cohen, R.E., 1995. Constraints on the crystalline structure of the inner core: mechanical instability of BCC iron at high pressure. *Geophys. Res. Lett.* 22, 125–128.
- Vočadlo, L., de Wijs, G.A., Kresse, G., Gillan, M.J., Price, G.D., 1997. First principles calculations on crystalline and liquid iron at Earth's core conditions. *Faraday Discuss.* 106, 205–217.
- Vočadlo, L., Brodholt, J., Alfe, D., Price, G.D., Gillan, M.J., 1999. The structure of iron under the conditions of the Earth's inner core. *Geophys. Res. Lett.* 26, 1231–1234.
- Vočadlo, L., Alfè, D., Gillan, M.J., Wood, I.G., Brodholt, J.P., Price, G.D., 2003. Possible thermal and chemical stabilization of body centred-cubic iron in the Earth's core. *Nature* 424, 536–539.
- Vočadlo, L., Wood, I.G., Gillan, M., Brodholt, J., Dobson, D.P., Price, G.D., Alfè, D., 2008a. The stability of bcc-Fe at high pressures and temperatures with respect to tetragonal strain. *Phys. Earth Planet. Inter.* 170, 52–59.
- Vočadlo, L., Wood, I.G., Alfè, D., 2008b. Ab initio calculations on the free energy and high  $P$ – $T$  elasticity of face-centred-cubic iron. *Earth Planet. Sci. Lett.* 268, 444–449.
- Wang, Y., Perdew, J., 1991. Correlation hole of the spin-polarized electron gas, with exact small-wave-vector and high-density scaling. *Phys. Rev. B* 44, 13,298–13,307.